RES MILITARIS Social Science Journal

Connections between a replaceable coupling beam and a double skin composite shear wall exhibit seismic activity

Avadhesh maurya, Satish Parihar, Vaibhav Dubey
Faculty of Engineering & Technology, Rama University, Mandhana, Kanpur, U.P, India
Email Id: er.avadhesh.civil@gmail.com

ABSTRACT

To maximise the effectiveness of the hybrid coupled wall system, a special connection between replacement coupling beams (RCB) and double skin composite shear walls (DSCSWs) is designed. For structural safety, the RCB-to-DSCSW link's seismic design is essential. This research examines the seismic behaviour of RCB-to-DSCSW couplings. Reversed cyclic stress was applied to two specimens with varied embedded rebar arrangement schemes and one specimen with an embedded steel I-beam. All of the specimens failed in the same manner, primarily as a result of concrete crushing at both ends of the joint, weld tensile fracture, and localised buckling of the steel faceplate. The strength and ductility of connections were significantly impacted by concrete crushing and weld tensile fracture. The concrete was swiftly crushed and the connection specimens reached their maximum load capacity at the current or next stage of weld tensile fracture. Compared to RC constructions, all of the specimens showed lower ductility coefficients. Additionally, these two varieties of embedded rebar connections have equivalent mechanical properties. The connection between the steel I-beams is more initially stiff. With the same rotation of loading, the steel beam's total energy consumption increased. The simplified mechanical model and equations for calculating connection bearing capacity were then developed based on the stress distribution of each component.

Keyword: Replacement coupling beam (RCB) and double skin composite shear walls (DSCSWs)

1. INTRODUCTION

The shear wall's lateral shear resistance is a critical safety consideration when designing high or super-high buildings. As the lateral resistances of typical reinforced concrete (RC) buildings grow, the cross-section size of shear walls expands, resulting in a rapid increase in structural weight and magnified seismic reactions. Double skin composite shear walls (DSCSWs) have recently been developed as an alternate answer to this challenge, and their seismic performance has been extensively researched. These pioneer investigations demonstrate that DSCSWs may efficiently regulate the self-weight of high-rise structures and display good seismic performances with reasonable construction procedures. As a result, DSCSWs have proven popular as lateral-force-resisting structural components in high-rise structures such as the Yancheng TV Tower and the China ZUN Tower. Different DSCSWs are typically used in high-rise structures to produce a shear-wall core utilising coupling beams.

2. MATERIALS AND METHODOLOGY

2.1 Testing program

2.1.1 Fabrication of specimens

Steel plate welds should avoid areas of high stress to avoid the influence of weld fracture on connection strength. To optimise the edge column manufacturing process, utilise the cold rolling method instead of the welding technique to create U-plate and avoid the effect of weld quality on joint strength. DSCSW manufacturing typically consists of two major tasks: steel plate preparation and concrete casting. As illustrated in Fig. 2, the fabrication process consists of four major processes based on the characteristics of each section of the structure.

Step 1: Form the edge of the wall with a welding steel plate (U-shape plate), Welding the embedded section to the U-shaped plate is the second step.

Step 3: Weld the interior steel plate to the U-shape plate to create an edge column.

Step 4: Weld the two connecting edge column faceplates.

Step 5: Attach the studs.

Step 6: Fixing the steel skeleton of the wall.

Step 7: Pouring the foundation concrete.

Step 8: Pouring the concrete for the top loading beam and the wall.

Allow adequate room during the design process for the coarse aggregate to move through smoothly. Furthermore, while casting concrete in the connection region, it should be completely vibrated and examined with equipment, such as the hammering technique, on a timely basis.

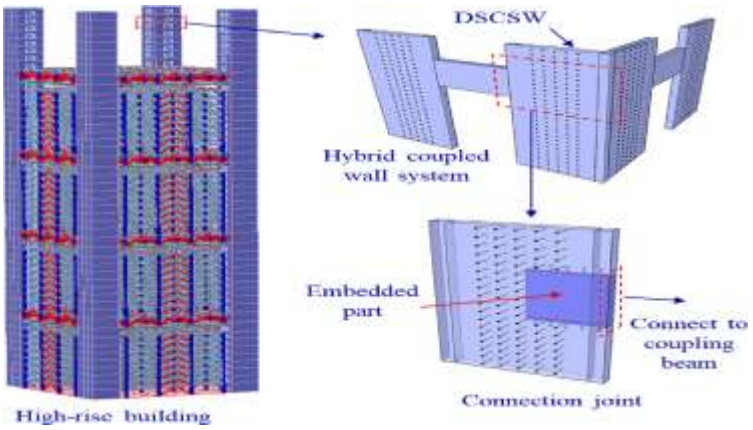

Fig. 1. Applications of RCB to DSCSW connection.

(a) Fabrication of edge column (b) Fabrication of wall steel skeleton

(c) Fixing wall skeleton and casting concrete of foundation (d) Casting concrete of wall and top beam

Fig. 2. Fabrication process of the Specimens.

2.1.2 Details of specimens

The prototype structure is a 55.2 m tall 18-story frame-shear wall construction. Three 2/3 sized specimens with distinct connections (CJ-1 CJ-3) are created for this investigation. Figure 3 depicts the specimens' 3D geometric features. All DSCSWs have the same cross-sectional dimensions, which are 1250 mm 125 mm 3000 mm in length breadth height. The steel plates and end plates of the embedded segments are 5 mm and 25 mm thick, respectively. CJ-1 employs the standard design approach for embedded segments, namely the bending moment and shear force coupling design. Except for the design idea of separating the bending moment and shear force, the features of CJ-2 are nearly identical to those of CJ-1. The prototype connecting beam is 3300 mm in length and 900 mm in height. Furthermore, the load point is positioned at the span's inverse bending point. The steel loading beam lb has a length of 1105 mm. The loading beam functions flexibly throughout the loading process since the focus of this article is on the strength of the embedded area. The shear connections between two faceplates are 10 mm diameter headed studs. The thickness, breadth, and height of the shear plate are 25 mm 160 mm 250 mm. The bolts that were welded to the shear plate have a diameter of 20 mm to prevent sliding between the shear plate and the concrete.

2.1.3 Material

Three 150×150×150 mm^3 cubes are manufactured for compression testing during the concrete casting process in order to determine their 28-day compressive strength. These cubes' average compressive strength (f_{cu}) is 42 MPa, with a standard variation of 4.97 MPa.

The mild steel Fe 250 is used to make specimen steel plates. Fe 415 steel is used to make the rebars in sample CJ-1, CJ-2, and CJ-3. Table 1 displays their mechanical qualities

(a) Overall view of DSCSW

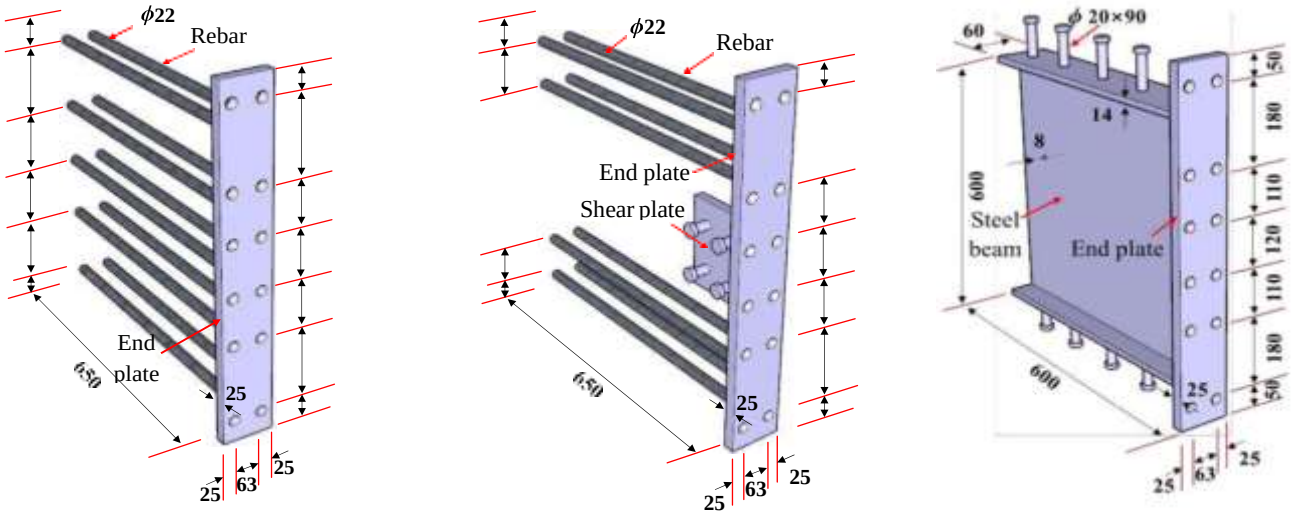

(b) CJ-1 (b) CJ-2 (b) CJ-3

Fig. 3. Dimension of DSCSW [illegible] segments

2.1.4 Measurement and Instr

During the testing, the reaction [illegible] ains of the specimen are measured. The specimens are being loade[illegible] measuring the lateral and vertical response forces. In order to m[illegible] s of DSCSWs at various heights, nine LVDTs (D5–D8 and D11) [illegible] A pair of crossing LVDTs, D[illegible] used to monitor the shear deformation of the embedded area of the DSCSW. [illegible] culated using Eq.

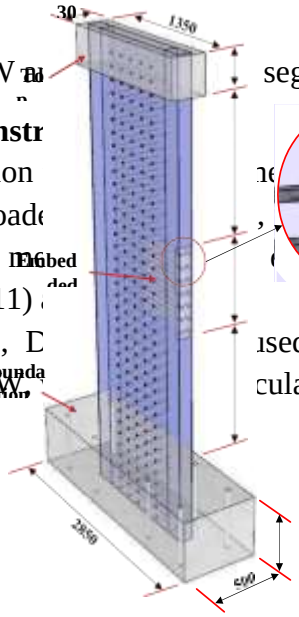

$$\theta = \frac{\left[\frac{D_2 + D_1}{2} - D_9\right]}{l_b}$$

$$\gamma = \frac{\alpha_1 + \alpha_2}{2} = \frac{\sqrt{b^2 + h^2}}{2bh}(\delta_2 - \delta_1)$$

Where, l_b = length of loading beam,
δ1 and δ2 = displacement changes on the two diagonals in the shear deformation region (D12 and D13),
b = width of the shear deformation region
h = height of the shear deformation region

3. RESULTS AND DISCUSSION

3.1 Damage and failure mode

The failure mode and failure progression are the same for all of the tested DSCSWs. The bearing capacity significantly decreased as a result of the specimens CJ-1, CJ-2, and CJ-3 gradually failing due to faceplate local buckling, weld tensile fracture, and concrete crushing. The following is a summary of the observed behaviours:

3.1.1 CJ-1

(1) Faceplate buckling occurs in the two end areas during the loading cycle of 0.012/0.009 rad, as illustrated in fig. 6(a). The specimen also reaches its maximum lateral shear resistance in the direction of positive stress.

(2) As shown in fig. 6(b), the welding of the face-plate at the two end areas fractures during the loading cycle of 0.019/0.018 rad, with the maximum fracture length being almost 53 mm. The specimen also reaches its maximum lateral shear resistance in the direction of negative stress.

(3) The loading force drops to 0.66/0.65 times the peak resistances in the two loading directions at the loading cycle of 0.041/0.035 rad. As depicted in fig. 6(c), the longest fracture length of the faceplate extends about to 124 mm, and the concrete crushing at the upper and lower of the connection also occurs there.

3.1.2 CJ-1

(1) Faceplate buckling occurs in the two end areas during the loading cycle of 0.0104 / 0.0096 rad, as illustrated in fig. 7(a).

(2) The welding of the faceplate at the two end areas fractures during the loading cycle of 0.0153/0.0155 rad, with the maximum fracture length being almost 112 mm, as shown in fig. 7(b). The specimen also reaches its maximum load resistance in two different loading directions.

(3) The loading force drops to 0.82/0.86 times the peak resistances in the two loading directions at the loading cycle of 0.0273/ 0.0344 rad.

3.1.2 CJ-3

(1) Faceplate buckling occurs in the two end areas during the loading cycle of 0.0123 / 0.0094 rad, as illustrated in fig. 8(a). In the direction of positive loading, the connection's vertical shear resistance peaked.

(2) The weld of the faceplate in the upper and lower areas at the intersection of the shear wall and loading beam ruptured at the loading cycle of 0.0208/0.0178 rad. The longest fracture was 53 mm in length. Additionally, as can be seen in fig. 8(b), the connection reached its maximum load resistance in the negative loading direction.

(3) The loading force dropped to 0.66/0.65 times the peak resistance in the positive/negative direction during the loading cycle of 0.0410/ 0.0354 rad. As can be seen in fig. 8(c), the concrete was crushed, and the faceplate of the wall had the longest fracture length at 124 mm.

Faceplate buckling, faceplate fracture, and concrete crushing are the principal failure mechanisms.

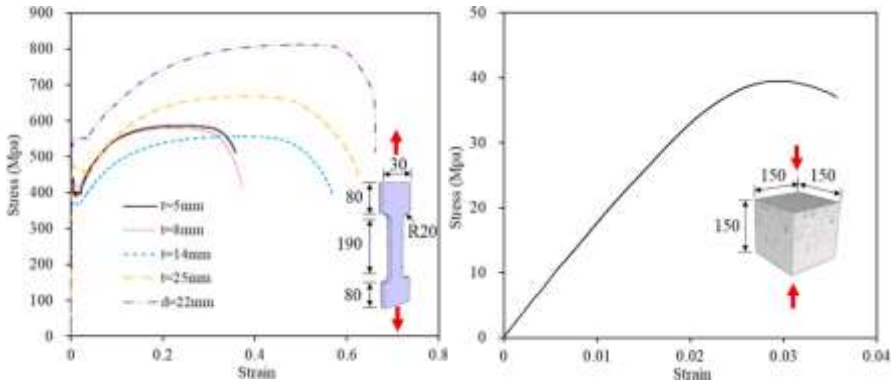

(a) Stress- strain curve of steel plate (b) Stress- strain curve of concrete

Fig. 4. Material test of steel plate and concrete

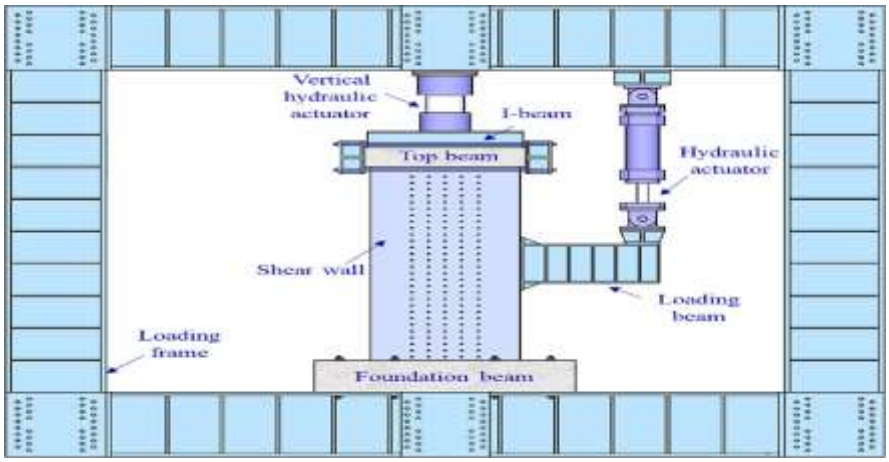

Fig. 5. Loading frame front view.

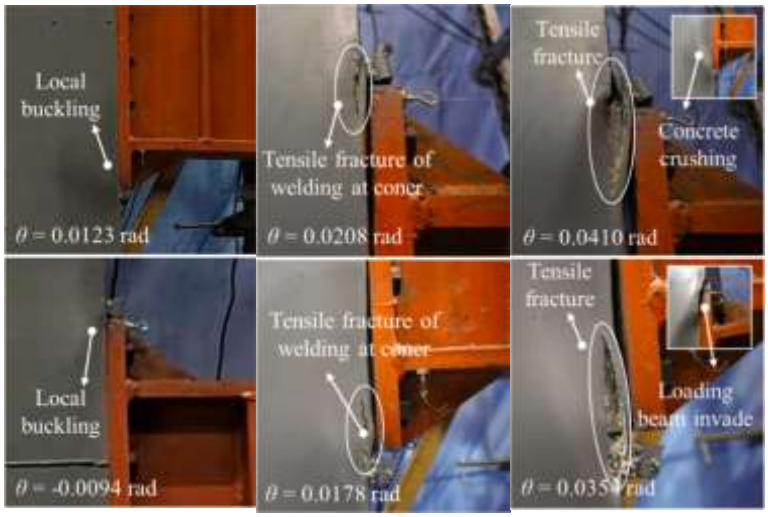

(a) (b) (c)

Fig. 6. Failure modes of CJ-1.

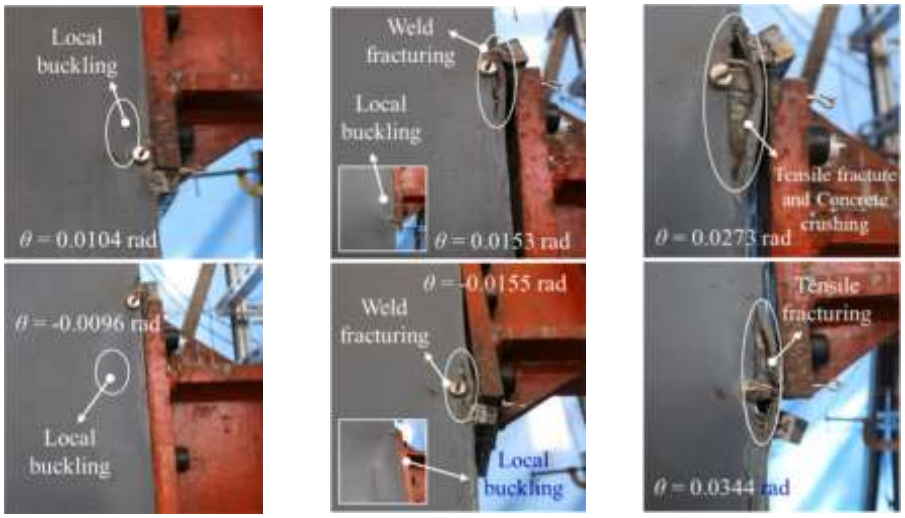

(a) (b) (c)

Fig. 7. Failure modes of CJ-2.

(a) (b) (c)

Fig. 8. Failure modes of CJ-3

4. CONCLUSION

This study looked at the seismic behaviours of three connections between the RCB and the DSCSW that included various sorts of embedded segments. Based on the test findings, it is possible to infer the subsequent conclusions:

1) By combining the strength of the steel plate and the embedded segment to withstand the external load, three types of RCB to DSCSW connections were proposed.

2) The neutral axis was quite near to the middle row rebars of CJ-1 and the shear plate in CJ-2, which had a little bearing capacity impact. Therefore, the two connections, CJ-1 and CJ-2, have comparable mechanical characteristics.

3) The ductility coefficients u of CJ-1, CJ-2, and CJ-3 were generally similar (2.30 to 3.85), and the initial stiffness with embedded steel beam connection was the greatest. Under the same stress level, CJ-3 has a higher capability for dissipating hysteretic energy than the others.

4) The theoretical calculation model and formula of the tested RCB to DSCSW connectors' bearing capacity were offered. The peak load carrying capacity of the RCB to DSCSW link under seismic stresses may be reasonably estimated using the provided theoretical models, which are conservative in nature.

REFERENCES

[1] Building Code Requirements for Structural Concrete and Commentary, An ACI Standard, reported by ACI Committee 318, American Concrete Institute, (2002).

[2] El-Tawil S, Harries KA, Fortney PJ, Shahrooz BM, Kurama Y. Seismic design of hybrid coupled wall systems: state of the art. J Struct Eng 2010;136(7):755–69.

[3] El-Tawil S, Harries KA. Recommendations for seismic design of hybrid coupled walls. Struct Eng Res Front ASCE 2007:1–10.

[4] Wang YY. Lessons learnt from building damages in the Wenchuan earthquake: seismic concept design of buildings[J]. J Build Struct 2008;29(4):20–5. in Chinese.

[5] Carpenter LD, Naeim F, Lew M, Youssef NF, Rojas F, Saragoni GR, et al. Performance of tall buildings in Viña del Mar in the 27 February 2010 offshore Maule, Chile earthquake. Struct Des Tall Spec Build 2011.

[6]